Pseudogap behaviour in $Bi_2Ca_2SrCuO_8$: Results of Generalized Dynamical Mean-Field Approach

E.Z.Kuchinskii[1], I.A.Nekrasov[1], Z.V.Pchelkina[2], M.V.Sadovskii[1]

[1] *Institute for Electrophysics, Russian Academy of Sciences, Ekaterinburg, 620016, Russia*
[2] *Institute for Metal Physics, Russian Academy of Sciences, Ekaterinburg, 620219, Russia*

Pseudogap phenomena are observed for normal underdoped phase of different high-T_c cuprates. Among others $Bi_2Sr_2CaCu_2O_{8-\delta}$ (Bi2212) compound is one of the most studied experimentally. To describe pseudogap regime in Bi2212 we employ novel generalized *ab initio* LDA+DMFT+$\Sigma_{\mathbf{k}}$ hybrid scheme. This scheme based on the strategy of one of the most powerfull computational tool for real correlated materials: local density approximation (LDA) + dynamical mean-field theory (DMFT). Here conventional LDA+DMFT equations are supplied by an additional (momentum dependent) self-energy $\Sigma_{\mathbf{k}}$ in the spirit of our recently proposed DMFT+$\Sigma_{\mathbf{k}}$ approach, accounting for pseudogap fluctuations. In the present model $\Sigma_{\mathbf{k}}$ describes non-local correlations induced by short-ranged collective Heisenberg-like antiferromagnetic spin fluctuations. The effective single impurity problem of the DMFT is solved by numerical renormalization group (NRG). Material specific model parameters for effective $x^2 - y^2$ orbital of Cu-3d shell of Bi2212 compound, e.g. the values of intra- and interlayer hopping integrals between different Cu sites, local Coulomb interaction U and pseudogap potential Δ were obtained within LDA and LDA+DMFT. Here we report theoretical LDA+DMFT+$\Sigma_{\mathbf{k}}$ quasiparticle bands dispersion and damping, Fermi surface renormalization, momentum anisotropy of (quasi) static scattering, densities of states, spectral densities and angular resolved photoemission (ARPES) spectra accounting for pseudogap and bilayer splitting effects for normal (slightly) underdoped Bi2212 (δ=0.15). We show that LDA+DMFT+$\Sigma_{\mathbf{k}}$ successfully describes strong (pseudogap) scattering close to Brillouin zone boundaries. Our calculated LDA+DMFT+$\Sigma_{\mathbf{k}}$ Fermi surfaces and ARPES spectra in presence of the pseudogap fluctuations are almost insensitive to the bilayer splitting strength. However, our LDA-calculated value of bilayer splitting is found to be rather small to describe experimentally observed peak-dip-hump structure. Results obtained are in good semiquantitative agreement with various recent ARPES experiments.

I. INTRODUCTION

Pseudogap state is the major anomaly of the normal state of copper oxides, commonly believed to be most relevant for the understanding of the physical nature of high-T_c superconductivity[1].

During the last decade experimental techniques of angular resolved photoemission spectroscopy (ARPES) has made a large progress. Sate-of-the-art high-T_c test compound for ARPES is $Bi_2Sr_2CaCu_2O_{8-\delta}$ (Bi2212) system. Thus a lot of experimental ARPES data is available for Bi2212 (for reviews see[2]). Several major experimental characteristics are derived from ARPES data like, for example, Fermi surfaces (FS), quasiparticle band dispersions and damping, and even self-energy lineshapes[2]. A number of interesting physical anomalies were discovered in normal underdoped phase of Bi2212: pseudogap formation, shadow bands and bilayer splitting of FS[2]. These phenomena abounds in theories and there are still no definite point of view about their physical origin. It is believed that all of these are quite relevant for the physics of high-temperature superconductors. The problem is much complicated by strong electronic correlations ever present in these compounds, making the standard band theory and Fermi liquid approaches doubtful.

In this work we show that taking into account short-range antiferromagnetic fluctuations resulting in pseudogap formation together with bilayer splitting effects is enough, in principle, to describe abovementioned experiments. To this end we employ novel hybrid *ab initio* LDA+DMFT+$\Sigma_{\mathbf{k}}$ computational scheme[15,16,17]. From one side this scheme inherits all the advantages of LDA+DMFT[3,4,5,6,7], i.e. the merger of first principle one-electron density functional theory within local densty approximation (DFT/LDA)[8,9] and the dynamical mean-field theory (DMFT) for strongly correlated electrons[10,11,12,13,14]. On the other side our scheme allows one to account for non-local correlation effects introducing momentum dependent external self-energy preserving conventional DMFT equations[15,16,17]. To solve the effective single impurity problem of the DMFT we employ here the reliable numerical renormalization group approach (NRG)[18,19].

Such combined scheme is particularly suitable to describe electronic properties of real high-T_c materials at finite doping in the normal state. First, all material specific model parameters for physically relevant effective $x^2 - y^2$ orbital of Cu-3d shell are obtained from LDA computations. Second, undoped cuprates are antiferromagnetic Mott insulators with $U \gg W$ (U — value of local Coulomb interaction, W — bandwidth of non–interacting band), so that correlation effects are very important. Thus at finite doping (up to optimal doping) cuprates are typical strongly correlated metals. To this end DMFT stage in our computational scheme

takes these strong electronic correlations into account. To adopt LDA+DMFT to study the "antiferromagnetic" scenario of pseudogap formation in cuprates[1,20,21,22] **k**-dependent self-energy $\Sigma_{\mathbf{k}}$ describing non-local correlations induced by (quasi) static short-ranged collective Heisenberg-like antiferromagnetic (AFM) spin fluctuations is included[21,22].

Recently we applied DMFT+$\Sigma_{\mathbf{k}}$ approach to investigate formation of pseudogap for strongly correlated metallic regime of single-band Hubbard model on the square lattice[15,16,17]. At present there are several independent methods aimed to describe non-local effects beyond standard DMFT. Similar results about pseudogap formation in the 2d Hubbard model were already obtained within two-particle self-consistent approach[23], cluster DMFT extensions, such as the dynamical cluster approximation (DCA)[30,31] and cellular DMFT (CDMFT)[23,24,27,28], CPT[25,26,36] and via the model of two interacting Hubbard sites self-consistently embedded in a bath[32]. The EDMFT was employed to demonstrate pseudogap formation in the DOS due to dynamic Coulomb correlations[37]. Important progress was also made with weak coupling approaches for the Hubbard model[38] and functional renormalization group[33,34]. In several papers pseudogap formation was described in the framework of the t-J model[39]. A more general scheme for the inclusion of non-local corrections was also formulated within the so called GW extension to DMFT[40,41]. Dynamical vertex approximation to study Mott-Hubbard transition in presence of non-local antiferromagnetic correlations was proposed[42]. Chain-DMFT extension was used to investigate breakup of the Fermi surface near Mott transition for quasi 1d Hubbard model[43].

The paper is organized as follows. In section II we present a short introduction into an *ab initio* self-consistent generalized combined LDA+DMFT+$\Sigma_{\mathbf{k}}$ scheme to account for short-rang AFM correlations. Section III contains Bi2212 material specific information: LDA calculated band structure and details on some model parameters calculations. Results and a discussion of LDA+DMFT+$\Sigma_{\mathbf{k}}$ computations for Bi2212 are presented in the sections IV and V.

II. COMPUTATIONAL METHOD

A. Introduction of the length scale into DMFT: DMFT+$\Sigma_{\mathbf{k}}$ approach

To introduce spatial length scale into conventional DMFT method[10,11,12,13,14] recently we proposed generalized DMFT+$\Sigma_{\mathbf{k}}$ approach[15,16,17]. The major assumption of our approach is that the lattice and Matsubara "time" Fourier transform of the single-particle Green function can be written as

$$G(\omega, \mathbf{k}) = \frac{1}{i\omega + \mu - \varepsilon(\mathbf{k}) - \Sigma(\omega) - \Sigma_{\mathbf{k}}(\omega)}, \quad (1)$$

where $\Sigma(\omega)$ is the *local* self-energy of DMFT, while $\Sigma_{\mathbf{k}}(\omega)$ is some momentum dependent part. Interference effects between these parts are neglected. Advantage of our generalized DMFT+$\Sigma_{\mathbf{k}}$ approach is additive form of self-energy in Eq. (1)[15,16,17]. It allows one to keep the set of self-consistent equations of standart DMFT[10,11,12,13,14]. However there are two distinctions. First, on each DMFT iteration we recalculate corresponding **k**-dependent self-energy $\Sigma_{\mathbf{k}}(\mu, \omega, [\Sigma(\omega)])$ within some (approximate) scheme, taking into account interactions with collective modes or order parameter fluctuations. Second, the local Green's function of effective impurity problem is defined as

$$G_{ii}(\omega) = \frac{1}{N} \sum_{\mathbf{k}} \frac{1}{i\omega + \mu - \varepsilon(\mathbf{k}) - \Sigma(\omega) - \Sigma_{\mathbf{k}}(\omega)}, \quad (2)$$

at each step of the standard DMFT procedure.

Eventually, we get the desired Green function in the form of (1), where $\Sigma(\omega)$ and $\Sigma_{\mathbf{k}}(\omega)$ are those appearing at the end of our iteration procedure.

To calculate $\Sigma_{\mathbf{k}}(\omega)$ for an electron moving in the random field of pseudogap fluctuations (assumed to be (quasi) static and Gaussian, which is valid at high enough temperatures[21,22]) with dominant scattering momentum transfers of the order of characteristic vector $\mathbf{Q} = (\pi/a, \pi/a)$ (a - lattice spacing) of AFM fluctuations ("hot spots" model[1]), we use the following recursion procedure proposed in Refs.[21,22]

$$\Sigma_{\mathbf{k}}(\omega) = \Sigma_{n=1}(\omega, \mathbf{k}), \quad (3)$$

where

$$\Sigma_n(\omega, \mathbf{k}) = \Delta^2 \frac{s(n)}{i\omega + \mu - \Sigma(\omega) - \varepsilon_n(\mathbf{k}) + i n v_n \kappa - \Sigma_{n+1}(\omega, \mathbf{k})}. \quad (4)$$

The quantity Δ characterizes the pseudogap energy scale and $\kappa = \xi^{-1}$ is the inverse correlation length of short range SDW fluctuations, $\varepsilon_n(\mathbf{k}) = \varepsilon(\mathbf{k} + \mathbf{Q})$ and $v_n = |v^x_{\mathbf{k}+\mathbf{Q}}| + |v^y_{\mathbf{k}+\mathbf{Q}}|$ for odd n, while $\varepsilon_n(\mathbf{k}) = \varepsilon(\mathbf{k})$ and $v_n = |v^x_{\mathbf{k}}| + |v^y_{\mathbf{k}}|$ for even n with $v^{x,y}(\mathbf{p})$ determined by usual momentum derivatives of the "bare" dispersion $\varepsilon(\mathbf{k})$, while $s(n)$ represents a combinatorial factor, determining the number of Feynman diagrams[21,22].

For the (Heisenberg) spin structure of interaction with spin fluctuations in "nearly antiferromagnetic Fermi–liquid" (spin–fermion (SF) model of Ref.[21]) spin-conserving scattering processes obey commensurate combinatorics, while spin–flip scattering is described by diagrams of incommensurate type ("charged" random field in terms of Ref.[21]). In this model combinatorial factor $s(n)$ acquires the following form[21]

$$s(n) = \begin{cases} \frac{n+2}{3} & \text{for odd } n \\ \frac{n}{3} & \text{for even } n. \end{cases} \quad (5)$$

Obviously, with this procedure we introduce an important length scale ξ not present in conventional DMFT.

Physically this scale mimics the effect of short-range (SDW) fluctuations within fermionic "bath" surrounding the effective Anderson impurity of the DMFT. We expect that such a length-scale dependence will lead to a kind of competition between local and non-local physics.

Though we prefer to consider both parameters Δ and ξ as phenomenological (to be determined by fitting experiments)[16], one can in principle calculate these from microscopic model at hand. For example, using the two-particle self-consistent approach of Refs.[23,45] with the approximations introduced in Refs.[21,22], we derived within the standard Hubbard model the following microscopic expression for Δ[16]

$$\Delta^2 = U^2 \frac{<n_{i\uparrow}n_{i\downarrow}>}{n^2} < (n_{i\uparrow} - n_{i\downarrow})^2 >, \qquad (6)$$

where we consider only scattering by antiferromagnetic spin fluctuations. The different local quantities – total density n, local densities $n_{i\uparrow}$, $n_{i\downarrow}$ and double occupancy $< n_{i\uparrow}n_{i\downarrow} >$ – can easily be calculated within the standard DMFT[13]. A detailed derivation of (6) is presented in the Appendix B of Ref.[16]. Corresponding microscopic expressions for the correlation length $\xi = \kappa^{-1}$ can also be derived within the two–particle self–consistent approach[23,45]. However, we expect these results for ξ to be less reliable, because this approach is valid only for relatively small (or medium) values of U/t, as well as for purely two-dimensional case, neglecting quasi-two-dimensional effects, obviously important for cuprates. Actually, our calculation experience shows that all the results obtained below are rather weakly dependent on the values of ξ from the experimentally relevant[1] interval of $(5 \div 10)a$.

B. Bilayer splitting effects: LDA+DMFT+$\Sigma_{\mathbf{k}}$ formulation

To perform *ab initio* calculations for Bi2212 system we employ LDA+DMFT strategy proposed in Refs.[3,4,5,6,7]. Necessary bare band dispersion for effective physically relevant Cu-3d $x^2 - y^2$ orbital in a tight-binding representation is

$$
\begin{aligned}
\varepsilon(\mathbf{k}) = \quad & -2t \quad (\cos k_x a + \cos k_y a) \\
& -4t' \quad \cos k_x a \cos k_y a \\
& -2t'' \quad (\cos 2k_x a + \cos 2k_y a) \\
& -2t''' \quad (\cos k_x a \cos 2k_y a + \cos 2k_y a \cos k_y a).
\end{aligned}
\qquad (7)
$$

Here t, t', t'', t''' are hopping integrals within first four coordination spheres. Tight-binding equation for interlayer dispersion is taken in the form

$$t_\perp(\mathbf{k}) = \frac{t_\perp}{4}(\cos k_x a - \cos k_y a)^2 \qquad (8)$$

given in Ref.[46] with bilayer splitting equal to $2t_\perp$.

Since account of bilayer splitting (BS) effects in Bi2212 requires essentially two-band model we introduce bare

Hamiltonian in reciprocal space as the following matrix over (bonding and antibonding) band indices

$$\hat{\mathbf{H}}(\mathbf{k}) = \begin{pmatrix} \varepsilon(\mathbf{k}) & t_\perp(\mathbf{k}) \\ t_\perp(\mathbf{k}) & \varepsilon(\mathbf{k}) \end{pmatrix}. \qquad (9)$$

The local Green's function is now also a matrix

$$\hat{\mathbf{G}}(\omega) = \frac{1}{N} \sum_{\mathbf{k}} \left(i\omega - \hat{\mathbf{H}}(\mathbf{k}) - (\Sigma(\omega) + \Sigma_{\mathbf{k}}(\omega))\hat{\mathbf{I}} \right)^{-1}. \qquad (10)$$

where we have assumed self-energies to be diagonal. In the following we would like to keep the DMFT part of the problem just a single-band task. This can be achieved taking the diagonal element of (10)

$$\widetilde{G}(\omega) = \frac{1}{N} \sum_{\mathbf{k}} \frac{G^{-1}(\omega, \mathbf{k})}{(G^{-1}(\omega, \mathbf{k}))^2 - (t_\perp(\mathbf{k}))^2}, \qquad (11)$$

where $G(\omega, \mathbf{k})$ is given by (1). This local Green's function $\widetilde{G}(\omega)$ (which includes additive self-energy contributions) determines now our effective single Anderson impurity problem. One should remark since we work with the single-band problem there is no need for double counting correction between LDA and DMFT.[5]

III. LDA BAND STRUCTURE OF BI2212 AND EFFECTIVE MODEL PARAMETERS

The Bi2212 compound has tetragonal bcc crystal lattice with symmetry space group I4/mmm[47,48,49]. Main structural motif for this compound is two CuO_2 layers displaced close to each other in the unit cell. Using crystal structure data of Ref.[47] we performed LDA calculations of electronic band structure within the linearized muffin-tin orbital (LMTO) basis set[50]. Obtained band structure is in agreement with the one of Ref.[47].

In Fig. 1 one-electron LDA band dispersion along BZ symmetry lines for Bi2212 is shown. Gray lines correspond to all-band Hamiltonian. To extract physically interesting partially filled $x^2 - y^2$ orbital of Cu-3d shell Wannier functions projecting method[51] in the LMTO framework[52] was applied. Corresponding dispersion of effective $x^2 - y^2$ orbital is displayed in Fig. 1 as a black line.

To set up the LDA+DMFT+$\Sigma_{\mathbf{k}}$ lattice problem (2) one needs to calculate transfer integrals t, t', t'', t''' and $t_\perp$ for tight-binding expressions (7) and (8). On the basis of Wannier function projecting[51] we performed computation of corresponding hopping integrals with its LMTO realization[52]. Obtained values for intra- and interlayer hybridization between $x^2 - y^2$ orbital of different Cu-sites are listed in the Table I. Values of t, t', t'', t''' we present are somewhat larger than those extracted from ARPES experiment[53]. On the other hand our value of $t_\perp$ is much smaller than experimental one $t_\perp^{exp}$=0.083 eV[53]. At the same time our calculated value of $t_\perp$ is in good agreement

with other band structure results reported[54]. Taking into account large difference between $t_\perp$ and $t_\perp^{exp}$ further we provide LDA+DMFT+$\Sigma_{\mathbf{k}}$ results for both these values.

The value of local Coulomb interaction U for $x^2 - y^2$ orbital was obtained via constrained LDA method[55]. To screen this $x^2 - y^2$ orbital we used the rest of the Cu-3d shell of our selected site, neighbouring inplane Cu sites and also Cu sites from closest CuO$_2$ layer. The value found is U=1.51 eV (Table I).

Pseudogap potential Δ (see Eq. (6)) was obtained as described in Ref.[16] using LDA+DMFT(NRG) to calculate set of occupancies entering (6) (instead of DMFT(QMC) used in Ref.[16]). For given values of hopping integrals and U value with hole doping level $\delta = 0.15$ our Δ equals 0.21 eV. The value of correlation length ξ is always taken to be equal to 5 lattice constants which is a typical experimental value[1]. Temperature comes through NRG part of our scheme and is always taken to be ~255 K. This completes the set of necessary model parameters to start LDA+DMFT+$\Sigma_{\mathbf{k}}$ computations for Bi2212 (see Sec. II).

IV. RESULTS AND DISCUSSION

A. Bi2212 LDA+DMFT+$\Sigma_{\mathbf{k}}$ densities of states

Density of states (DOS) is calculated as

$$N(\omega) = -\frac{1}{\pi} \mathrm{Im} \widetilde{G}(\omega) \qquad (12)$$

where $\widetilde{G}(\omega)$ is defined by Eq. 11 analytically continued to real frequencies. In Fig. 2 we display LDA+DMFT and LDA+DMFT+$\Sigma_{\mathbf{k}}$ DOS for effective $x^2 - y^2$ orbital of Cu-3d. It is clearly seen that pseudogap fluctuations lead to formation of the pseudogap in DOS within 0.2 eV from the Fermi level. In our model this pseudogap is not tied to the Fermi level and it is not very pronounced for parameter values used here for Bi2212. It is also easy to find out that for all our DOS curves BS effects are most pronounced on the top of the van Hove singularity, which is about around -0.2 eV below the Fermi level (see also inset of Fig. 2 for details). Namely we calculate DOS for LDA value of BS 0.03 eV (gray curve) and experimental BS value of 0.083 eV (black line). For the latter case BS effects are obviously stronger. Dashed curves correspond to LDA+DMFT results for two different values of bilayer splitting. For LDA+DMFT+$\Sigma_{\mathbf{k}}$ DOS (solid curves) it is observed that BS effects become less pronounced (but still can be seen for the case of $t_\perp^{exp}$=0.083 eV). This is caused by the decrease of the life-time due to pseudogap fluctuations. Also van Hove singularity becomes slightly narrower here due to self-energy effects. Note that the shape of the pseudo gap in the DOS almost does not depend on BS effects.

B. Bi2212 LDA+DMFT+$\Sigma_{\mathbf{k}}$ qusiparticle dispersions and damping

For the case of finite temperature and interaction values we define quasiparticle dispersions via maxima positions of corresponding spectral functions $A(\omega, \mathbf{k})$

$$A(\omega, \mathbf{k}) = -\frac{1}{\pi} \mathrm{Im} \widetilde{G}(\omega, \mathbf{k}), \qquad (13)$$

where $\widetilde{G}(\omega, \mathbf{k})$ is defined by an expression under the sum in (11), analytically continued to real frequencies, with self–energies and chemical potential μ calculated self–consistently as described in Sec. II A.

In Figs. 3 and 4 we present LDA+DMFT and LDA+DMFT+$\Sigma_{\mathbf{k}}$ quasiparticle bands dispersions (crosses) for Bi2212 effective $x^2 - y^2$ orbital of Cu-3d shell along the symmetry lines in the Brillouin zone (BZ) for $t_\perp$ and $t_\perp^{exp}$. Background shows quasiparticle damping given by the imaginary part of additive $\Sigma(\omega) + \Sigma_{\mathbf{k}}(\omega)$ self-energy. The more intensive colour corresponds to the larger damping. In case of standard LDA+DMFT computations, neglecting non-local corrections (Fig. 3), one can clearly see that the damping is uniform over all BZ. This is due to local nature of conventional DMFT. Quasiparticles are well defined in narrow light region around zero energy (Fermi level).

When we introduce spatial inhomogeneity into DMFT bath within the LDA+DMFT+$\Sigma_{\mathbf{k}}$ approach the damping appears to be much stronger and consequently non-uniform as seen in Fig. 4. Again quasiparticles are well defined close to the Fermi level. But now the contour plot of Im[$\Sigma(\omega) + \Sigma_{\mathbf{k}}(\omega)$] self-energy (damping) clearly shows so-called "shadow band" which looks like the quasiparticle band mirrored around the zero energy. In Fig. 4 we can also see pseudogap formation around X point. In our case shadow band is formed due to short-ranged AFM fluctuations. Close to X point BS effects are most pronounced. One can see that maxima of $A(\omega, \mathbf{k})$ belonging to the "shadow band" region are conserved only rather close to the X point, further away these maxima vanish due to large damping. In the middle of MG direction we observe preformation of AFM insulating gap in the cross point of quasiparticle and and "shadow" bands.

C. Bi2212 LDA+DMFT+$\Sigma_{\mathbf{k}}$ spectral functions

To plot spectral functions $A(\omega, \mathbf{k})$ (13) we choose $\mathbf{k}$-points along the 1/8-th part of the "bare" Fermi surface within the first quadrant of the Brillouin zone for given lattice spectra and filling. In Fig. 5 corresponding spectral functions for different strength of bilayer splitting are shown.

Close to the to nodal point (upper curve) spectral function in Fig. 5 has the typical Fermi–liquid behaviour, consisting of a rather sharp peak close to the Fermi level. Going to the antinodal point (lower curve) fluctuations

becomes stronger and shift the sharp peak out of the Fermi level down in energy. Simultaneously with the growth of fluctuation strength damping also grows, so the peak becomes less intensive and more broad. In the vicinity of the "hot–spot" (black line) the shape of $A(\omega, \mathbf{k})$ is completely modified. Now $A(\omega, \mathbf{k})$ becomes double–peaked and non–Fermi–liquid–like. Directly at the "hot spot", $A(\omega, \mathbf{k})$ has two peaks (second one is much less intensive) situated symmetrically around the Fermi level and splitted from each other by $\sim 1.5\Delta$[21,22].

For the case of $t_\perp^{exp}$ (right panel of Fig. 5) behaviour is similar to one for $t_\perp$ (upper panel of Fig. 5). However now bilayer splitting strength is big enough to be resolved. So the peak-dip-hump structure[2] is formed on the edges of pseudogap.

D. Bi2212 LDA+DMFT+$\Sigma_\mathbf{k}$ ARPES spectra

Knowing $A(\omega, \mathbf{k})$ (13) we are now of course in a position to calculate angle resolved photoemission (ARPES) spectra, which are the most direct experimental way to observe pseudogap in real compounds. For that purpose, we only need to multiply our results for the spectral functions with Fermi function at temperature 255 K. The resulting LDA+DMFT+$\Sigma_\mathbf{k}$ ARPES spectra are presented in Fig. 6. Again these spectra are drawn along 1/8 of non-interacting FS from antinodal (lower curve) to nodal point (upper curve). At the antinodal point we find well defined (sharp) quasiparticle peak close to the Fermi level. Moving towards the antinodal point the damping (widening) of this quasiparticle peak and its shift to higher binding energies are observed. Such behaviour is typically obtained experimentally[2]. To describe peak-dip-hump splitting resolved in experiment[2] we take $t_\perp^{exp}$=0.083 eV[53]. Indeed for $t_\perp^{exp}$ we get pronounced peak-dip-hump structure similar to experimental one[2]. It is recognized that our LDA-calculated $t_\perp$ is several times smaller and can not provide adequate description of the peak-dip-hump structure for ARPES data. Notice that the intensity of antibonding branch is higher than for bonding one. It is opposite in the experiment. We attribute this difference to the matrix elements effects which are not taken into account in the present work.

In Fig. 7 we show comparison of LDA+DMFT+$\Sigma_\mathbf{k}$ ARPES spectra and experimental one from Ref.[59] for Bi2212 measured along the Fermi surface. Here spectral functions displayed in Fig. 5 are multiplied with the Fermi function at experimental temperature T=140 K and convoluted with Gaussian to simulate experimental resolution of 16 meV.[59] All theoretical ARPES curves after multiplication and broadening are normalized to 1. Left and right panels of Fig. 7 correspond to the theoretical data for $t_\perp$ and $t_\perp^{exp}$ values. Both figures demonstrate semiquantitative agreement of our theoretical results with the experiment. Common trend for both panels is the damping of quasiparticle peak and its retreat to

higher binding energies as we move from nodal to antinodal region. Displacements of theoretical and experimental peaks on the left panel of Fig. 7 are in good quantitative agreement. However theoretical peaks are always a little bit sharper and narrower. Take notice that the left panel demonstrates no BS effects. On the right panel of Fig. 7 we found slightly better agreement of intensities due to bigger BS value $t_\perp^{exp}$. But for the $\mathbf{k}$-values between the "hot spot" and the antinodal point there we have some lack of spectral weight close to the Fermi level. Also for these $\mathbf{k}$-values we observe some reminiscence of the bilayer splitting. After all one can infer that BS effects do not change the line shape of our ARPES spectra significantly and for both cases we obtain rather satisfactory agreement with the experiment.

E. Bi2212 LDA+DMFT+$\Sigma_\mathbf{k}$ Fermi surface

In the following we characterize renormalized Fermi surfaces (FS) by intensity plots of spectral density at zero frequency $A(\omega = 0, \mathbf{k})$ (which for the free-electron case just follow the "bare" Fermi surface).

In the Figs. 8 and 9 we display thus defined LDA+DMFT and LDA+DMFT+$\Sigma_\mathbf{k}$ Fermi surfaces for Bi2212. LDA+DMFT FS has the LDA shape, as it should be within DMFT (see Fig. 8). Slight broadening close to the borders of BZ is because of BS effects. Non-zero width of FS (in contrast to LDA) comes from finite damping due to interaction and temperature. For LDA+DMFT+$\Sigma_\mathbf{k}$ FS (see Fig. 9) one can see significant "destruction" effects in the vicinity of the antinodal point induced by pseudogap fluctuations. From comparison of upper and lower panels of Fig. 9 one can conclude that for strongly correlated case BS effects alone are not enough to describe experimentally observed FS "destruction" close to the borders of BZ and formation of "Fermi arcs" around the nodal point, as observed in ARPES experiments[2]. We found that FS shape is rather insensitive to BS strength since pseudogap fluctuations are much stronger than bilayer splitting and hide it. Though BS at the BZ boundaries slightly amplifies pseudogap effects. Thus the account of pseudogap (AFM) fluctuations seems to be necessary to describe experimental picture.

F. Bi2212 LDA+DMFT+$\Sigma_\mathbf{k}$ anisotropy of static scattering

Strong anisotropy of (quasi) static scattering was observed in Bi2212 system in ARPES experiments in Refs.[57,58,59] and attributed to scattering by planar impurities[60,61]. Here we show that this effect can be naturally explained by (quasi) static scattering by pseudogap fluctuations.

Our LDA+DMFT+$\Sigma_\mathbf{k}$ calculated (quasi) static scattering defined as $a(\mathbf{k}) = \Sigma(0) + \Sigma_\mathbf{k}(0)$ is plotted in Fig. 9, together with experimental data of Refs.[58,59].

Here **k**-points are taken along 1/8 of non-interacting FS. We detect our results to mediate experimental data of Refs.[58,59], while the difference between latter remains itself unexplained.

In our opinion, anisotropy of (quasi) static scattering $a(\mathbf{k})$ naturally follows from anisotropic renormalization of electronic spectrum due to pseudogap fluctuations, which directly follows from our "hot spot" like model[21,22].

Despite overall behaviour is analogous to one obtained in the experiment there is a need for further studies of possible relevance of matrix elements effects in ARPES, as well as that of additional scattering by random static impurities[17].

V. CONCLUSION

Present investigation is aimed to describe pseudogap regime of high-T_c cuprate $Bi_2Sr_2CaCu_2O_{8-\delta}$ (Bi2212) from first principles. For this purpose we employ novel generalized *ab initio* LDA+DMFT+$\Sigma_{\mathbf{k}}$ hybrid scheme. This scheme based on the strategy of most powerfull computational tool for real correlated materials: local density approximation (LDA) + dynamical mean-field theory (DMFT). Here we supply conventional LDA+DMFT equations with an additional (momentum dependent) self-energy $\Sigma_{\mathbf{k}}$ in the spirit of our recently proposed DMFT+$\Sigma_{\mathbf{k}}$ approach. "External" self-energy $\Sigma_{\mathbf{k}}$ is chosen here to describe non-local dynamical correlations induced by short-ranged collective Heisenberg-like antiferromagnetic spin fluctuations (in static Gaussian approximation of Refs.[21,22]). Necessary Bi2212 material specific model parameters for effective $x^2 - y^2$ orbital of Cu-3d shell, e.g. the values of intra- and interlayer hopping integrals, local Coulomb interaction U and pseudogap potential Δ were calculated within LDA and LDA+DMFT. On the basis of LDA+DMFT+$\Sigma_{\mathbf{k}}$ computations we obtain densities of states, spectral functions $A(\omega, \mathbf{k})$ which allow one to visualize quasiparticle bands dispersion and damping, Fermi surface (FS), anisotropy of static scattering $a(\mathbf{k})$ and ARPES spectra accounting for pseudogap and bilayer splitting effects for normal (slightly) underdoped Bi2212 (δ=0.15). It is found that on the DOS level BS and pseudogap effects are separated in energy and hardly affect each other. We showed that LDA+DMFT+$\Sigma_{\mathbf{k}}$ describes strong scattering at Brillouin zone boundaries as pure manybody effect. LDA+DMFT+$\Sigma_{\mathbf{k}}$ Fermi surface in presence of the pseudogap fluctuations is almost insensitive to the BS strength. Thus the BS effects alone are not enough to describe the Fermi surface destruction (though amplifies it) and additional source of electron scattering is required (for example, AFM short-range fluctuations). The only place where BS effects play significant role is formation of the experimentally observed peak-dip-hump structure in ARPES spectra. To this end the LDA-calculated value of bilayer splitting is found to be rather small to describe this effect. Results obtained are in good semiqualitative agreement with various recent ARPES experiments.

At present there are several alternative points of view on the possible explanation of Fermi surface destruction, formation of shadow Fermi bands etc. Recently the analysis of the effect of three-dimensionality on the ARPES spectra was presented for Bi2212 in Ref.[62]. It was shown that in a quasi-2D system, the weak k_z-dispersion can lead to Fermi surface maps similar to those observed in the experiment. This FS broadening mechanism does not have the manybody origin. The authors of Ref.[63] have shown that shadow Fermi surface in Bi2212 can be interpreted as an intrinsic feature of the initial electronic spectrum arising from bulk, orthorhombic distortions located primarily in the BiO planes, but most definitely felt throughout the three-dimensional crystal. All these effects are not considered here thus remain for further investigations. Apparently, in a real system these mechanisms combine with those described above leading to a complete picture of electronic structure of Bi2212.

VI. ACKNOWLEDGEMENTS

[1] T. Timusk, B. Statt, Rep. Progr. Phys, **62**, 61 (1999); M.V. Sadovskii. Usp. Fiz. Nauk **171**, 539 (2001) [Physics – Uspekhi **44**, 515 (2001)].

[2] A. Damascelli, Z. Hussain, Z.-X. Shen, Rev. Mod. Phys. 75, 473 (2003); J.C. Campuzano, M.R. Norman, M. Randeria, In "Physics of Superconductors", Vol. II, ed. K. H. Bennemann and J. B. Ketterson (Springer, Berlin, 2004), p. 167-273; J. Fink, et al., cond-mat/0512307; X.J. Zhou, et al., cond-mat/0604284.

[3] V. I. Anisimov, A. I. Poteryaev, M. A. Korotin, A. O. Anokhin, and G. Kotliar, J. Phys. Cond. Matter **9**, 7359 (1997).

[4] A. I. Lichtenstein, M. I. Katsnelson, Phys. Rev. B **57**, 6884 (1998).

[5] I. A. Nekrasov, K. Held, N. Blümer, A. I. Poteryaev, V. I. Anisimov, and D. Vollhardt, Euro. Phys. J. B **18**, 55 (2000).

[6] K. Held, I. A. Nekrasov, G. Keller, V. Eyert, N. Blumer, A. K. McMahan, R. T. Scalettar, Th. Pruschke, V. I. Anisimov, and D. Vollhardt, Psi-k Newsletter **56**, 65 (2003) [psi-k.dl.ac.uk/newsletters/News_56/Highlight_56.pdf].

[7] K. Held, I. A. Nekrasov, N. Blümer, V. I. Anisimov, and D. Vollhardt, Int. J. Mod. Phys. B **15**, 2611 (2001); K. Held, I. A. Nekrasov, G. Keller, V. Eyert, N. Blümer, A. K. McMahan, R. T. Scalettar, T. Pruschke, V. I. Anisimov, and D. Vollhardt, available as cond-mat/0112079 (Published in *Quantum Simulations of Complex Many-Body Systems: From Theory to Algorithms*, eds. J. Grotendorst, D. Marks, and A. Muramatsu, NIC Series Volume 10 (NIC Directors, Forschunszentrum Jülich, 2002) p. 175-209 (ISBN 3-00-009057-6); A. I. Lichtenstein, M. I. Katsnelson, G. Kotliar, in *Electron Correlations and Materials Properties 2nd ed.*, edited by A. Gonis, Nicholis Kioussis and Mikael Ciftan, Kluwer Academic/Plenum, p. 428, New York (2002), available as cond-mat/0112079.

[8] W. Kohn and L. J. Sham, Phys. Rev. **140**, A1133 (1965); L. J. Sham and W. Kohn, Phys. Rev. **145**, 561 (1966).

[9] L. Hedin and B. I. Lundqvist, J. Phys. C **4**, 2064 (1971); U. von Barth and L. Hedin, *ibid.* **5**, 1629 (1972).

[10] W. Metzner and D. Vollhardt, Phys. Rev. Lett. **62**, 324 (1989).

[11] D. Vollhardt, in *Correlated Electron Systems*, edited by V. J. Emery, World Scientific, Singapore, 1993, p. 57.

[12] Th. Pruschke, M. Jarrell, and J. K. Freericks, Adv. in Phys. **44**, 187 (1995).

[13] A. Georges, G. Kotliar, W. Krauth, and M. J. Rozenberg, Rev. Mod. Phys. **68**, 13 (1996).

[14] G. Kotliar and D. Vollhardt, Physics Today **57**, No. 3 (March), 53 (2004).

[15] E.Z. Kuchinskii, I.A. Nekrasov, M.V. Sadovskii. JETP Lett. **82**, 198 (2005)

[16] M.V. Sadovskii, I.A. Nekrasov, E.Z. Kuchinskii, Th. Prushke, V.I. Anisimov. Phys. Rev. B **72**, 155105 (2005)

[17] E.Z. Kuchinskii, I.A. Nekrasov, M.V. Sadovskii, Low Temperature Physics **32** (2006) 528.

[18] K.G. Wilson, Rev. Mod. Phys. **47**, 773 (1975); H.R. Krishna-murthy, J.W. Wilkins, and K.G. Wilson, Phys. Rev. B **21**, 1003 (1980); *ibid.* **21**, 1044 (1980); for a comprehensive introduction to teh NRG see e.g. A.C. Hewson, *The Kondo Problem to Heavy Fermions* (Cambridge University Press, 1993).

[19] R. Bulla, A.C. Hewson and Th. Pruschke, J. Phys. – Condens. Matter **10**, 8365 (1998);

[20] D. Pines, ArXiv: cond-mat/0404151.

[21] J. Schmalian, D. Pines, B.Stojkovic, Phys. Rev. B **60**, 667 (1999).

[22] E. Z. Kuchinskii, M. V. Sadovskii, Zh. Eksp. Teor. Fiz. **115**, 1765 (1999) [(JETP **88**, 347 (1999)].

[23] A.-M.S Tremblay, B. Kyung, D. Senechal, Low Temperature Physics **32**, 561 (2006)

[24] G. Kotliar, S.Y. Savrasov, G. Palsson, G. Biroli, Phys. Rev. Lett. **87**, 186401 (2001); For periodized version (PCDMFT) see M. Capone, M. Civelli, S.S. Kancharla, C. Castellani, and G. Kotliar, Phys. Rev. B **69**, 195105 (2004).

[25] C. Gros, and R. Valenti, Annalen der Phys. **3**, 460 (1994).

[26] D. Senechal, D. Perez, and M. Pioro-Ladrie, Phys. Rev. Lett. **84**, 522 (2000); D. Senechal, D. Perez, and D. Plouffe, Phys. Rev. B **66**, 075129 (2002).

[27] B. Kyung, S.S. Kancharla, D. Senechal, A.-M.S. Tremblay, M. Civelli, G. Kotliar, ArXiv: cond-mat/0502565.

[28] M. Civelli, M. Capone, S.S. Kancharla, O. Parcollet, G. Kotliar, ArXiv: cond-mat/0411696.

[29] A. Kaminski, H. M. Fretwell, M. R. Norman, M. Randeria, S. Rosenkranz, U. Chatterjee, J. C. Campuzano, J. Mesot, T. Sato, T. Takahashi, T. Terashima, M. Takano, K. Kadowaki, Z. Z. Li, H. Raffy, Phys. Rev. B **71**, 014517 (2005).

[30] Th. Maier, M. Jarrell, Th. Pruschke and M. Hettler, Rev. Mod. Phys. **77**, 1027 (2005).

[31] Th.A. Maier, Th. Pruschke, and M. Jarrell, Phys. Rev. B **66**, 075102 (2002).

[32] T.D. Stanescu and P. Phillips, Phys. Rev. Lett. **91**, 017002 (2003).

[33] A.A. Katanin and A.P. Kampf, Phys. Rev. Lett. **93**, 106406 (2004)

[34] D. Rohe, W. Metzner, Phys. Rev. B**71**, 115116 (2005).

[35] D.K. Sunko, S. Barisic, Eur. Phys. J. B **46**, 269 (2005).

[36] D. Senechal and A.-M.S. Tremblay, Phys. Rev. Lett. **92**, 126401 (2004).

[37] K. Haule, A. Rosch, J. Kroha, P. Wölfle, Phys. Rev. Lett. **89**, 236402 (2002); Phys. Rev. B **68**, 155119 (2003).

[38] B. Kyung, V. Hankevich, A.-M. Dare, A.-M.S. Tremblay. Phys. Rev. Lett. **93**, 147004 (2004).

[39] P. Prelovsek and A. Ramsak, Phys. Rev. B **63**, 180506 (2001); P. Prelovsek, A. Ramsak, ArXiv: cond-mat/0502044.

[40] S. Biermann, F. Aryasetiawan, A. Georges, Phys. Rev. Lett. **90**, 086402 (2003).

[41] P. Sun, G. Kotliar, Phys. Rev. Lett. **92**, 196402 (2004).

[42] A. Toschi, A. A. Katanin, K. Held, cond-mat/0603100.

[43] C. Berthod, T. Giamarchi, S. Biermann, A. Georges, cond-mat/0602304.

[44] M. V. Sadovskii, Zh. Eksp. Teor. Fiz. **77**, 2070 (1979) [Sov.Phys.–JETP **50**, 989 (1979)].

[45] Y. M. Vilk, A.-M. S. Tremblay, J. Phys. I France **7**, 1309 (1997).

[46] Andersen O.K., Liechtenstein A.I., Jepsen O., Paulsen F., J. Phys. Chem. Solids, **56**, 1573 (1995).

[47] M. Hybertsen and L. Mattheiss, Phys. Rev. Lett. 60, 1661 (1988).

[48] J. M. Tarascon, et al., Phys. Rev. B 37, 9382 (1988).

[49] S. A. Sunshine, et al., Phys. Rev. B 38, 893 (1988).

[50] O. K. Anderson, Phys. Rev. B 12, 3060 (1975); H. L. Skriver, The LMTO Method (Springer-Verlag, New York, 1984).

[51] N. Marzari and D. Vanderbilt, Phys. Rev. B 56, 12847 (1997); W. Ku, et al., Phys. Rev. Lett. 89, 167204 (2002).

[52] V. I. Anisimov, et al., Phys. Rev. B 71, 125119 (2005).

[53] A.A. Kordyuk, S.V. Borisenko, M. Knupfer, and J. Fink, Phys. Rev. B **67**, 064504 (2003).

[54] A.A. Kordyuk, S.V. Borisenko, A.N. Yaresko, S.-L. Drechsler, H. Rosner, T.K. Kim, A. Koitzsch, K.A. Nenkov, M. Knupfer, J. Fink, R. Follath, H. Berger, B. Keimer, S. Ono, and Yoichi Ando, Phys. Rev. B **70**, 214525 (2004).

[55] O. Gunnarsson, O. K. Andersen, O. Jepsen, and J. Zaanen, Phys. Rev. B **39**, 1708 (1989).

[56] A.I. Liechtenstein, O. Gunnarsson, O.K. Andersen, R.M. Martin, Physical Review B **54** 12505, (1996).

[57] T. Valla, A.V. Fedorov, P.D. Johnson, Q. Li, G.D. Gu, N. Koshizuka, Phys. Rev. Lett. **85**, 828 (2000).

[58] A. Kaminski, H.M. Fretwell, M.R. Norman, M. Randeria, S. Rosenkranz, J.C. Campuzano, J. Mesot, T. Sato, T. Takahashi, T. Terashima, M. Takano, K. Kadowaki, Z.Z. Li, H. Raffy, ArXiv: cond-mat/0404385.

[59] A. Kaminski, H.M. Fretwell, M.R. Norman, M. Randeria, S. Rosenkranz, J.C. Campuzano, J. Mesot, T. Sato, T. Takahashi, T. Terashima, M. Takano, K. Kadowaki, Z.Z. Li, H. Raffy, Phys. Rev. B **71**, 014517 (2005).

[60] C.M. Varma, E.A. Abrahams, Phys. Rev. Lett. **86**, 4652 (2001).

[61] E. Abrahams, C.M. Varma, Proc. Natl. Acad. Sci. USA **97**, 5714 (2000).

[62] A. Bansil, M. Lindroos, S. Sahrakorpi, and R. S. Markiewicz, Phys. Rev. B **71**, 012503 (2005).

[63] A. Mans, I. Santoso, Y. Huang, W. K. Siu, S. Tavaddod, V. Arpiainen, M. Lindroos, H. Berger, V. N. Strocov, M. Shi, L. Patthey, and M. S. Golden, Phys. Rev. Lett. **96**, 107007 (2006).

Figures

FIG. 2: (Color online) LDA+DMFT (dashed lines) and LDA+DMFT+$\Sigma_{\mathbf{k}}$ (solid lines) densities of states for Bi2212 for LDA-calculated value of $t_\perp$=0.03 eV (black) and experimental value of $t_\perp^{exp}$=0.083 eV (gray) (Coulomb interaction U=1.51 eV, filling n=0.85, pseudogap potential Δ=0.21 eV, correlation length $\xi = 5a$). Inset shows magnified region around the Fermi level.

FIG. 3: (Color online) LDA+DMFT quasiparticle bands for Bi2212 (crosses) along BZ high symmetry directions for LDA-calculated value of $t_\perp$=0.03 eV (upper panel) and experimental value of $t_\perp^{exp}$=0.083 eV (lower panel) (Coulomb interaction U=1.51 eV, filling n=0.85). Zero of background (which is -$1/\pi$Im$\Sigma(\omega)$ - local DMFT self-energy) corresponds to zero damping.
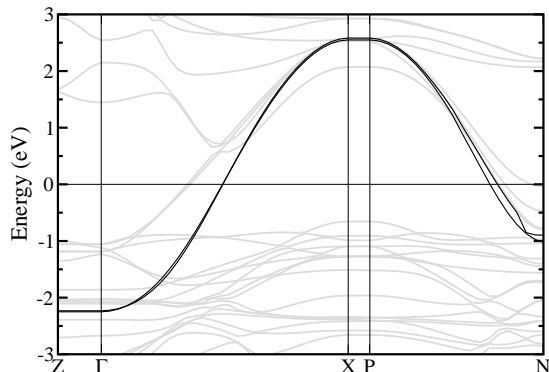

FIG. 1: Calculated within DFT/LDA Bi2212 band dispersions (gray lines) and effective $x^2 - y^2$ band of Cu-3d shell obtained by projection on Wannier functions (black lines). The Fermi level corresponds to zero.
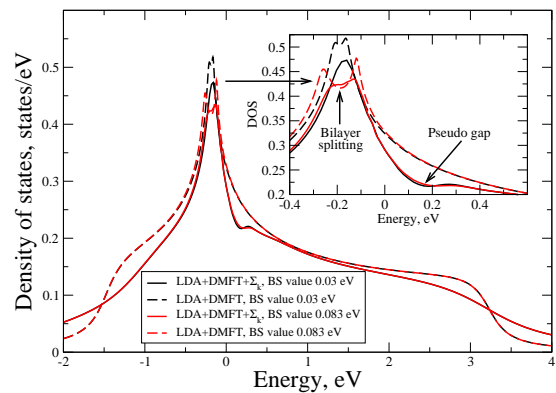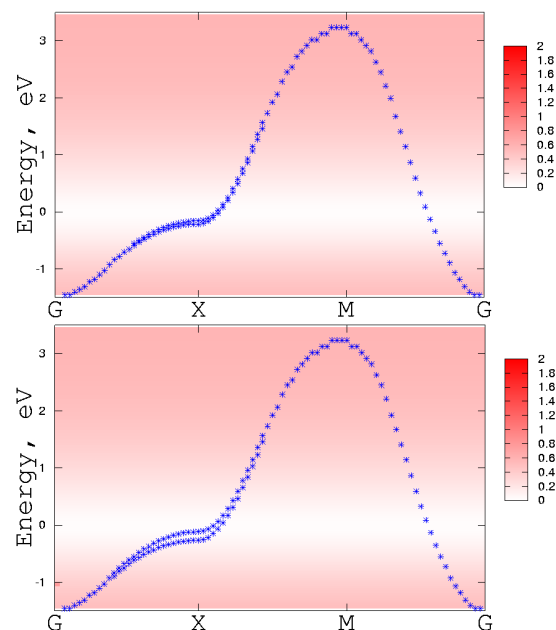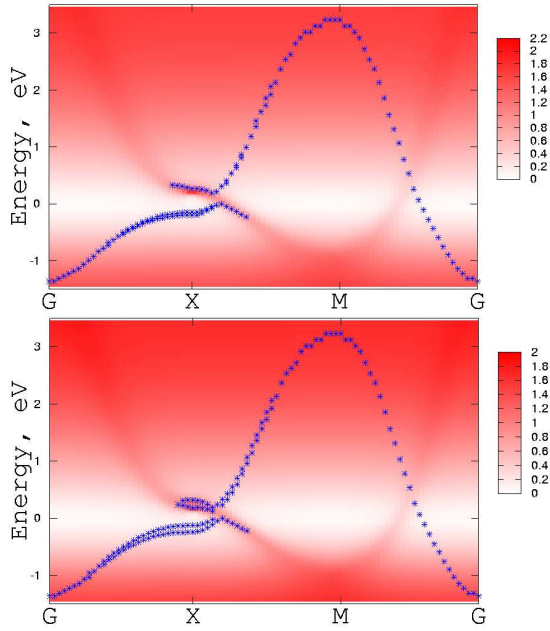
FIG. 4: (Color online) LDA+DMFT+$\Sigma_{\mathbf{k}}$ quasiparticle bands for Bi2212 (crosses) along BZ high symmetry directions for LDA-calculated value of $t_\perp$=0.03 eV (upper panel) and experimental value of $t_\perp^{exp}$=0.083 eV (lower panel) (Coulomb interaction U=1.51 eV, filling n=0.85, pseudogap potential Δ=0.21 eV, correlation length $\xi = 5a$). Zero of background (which is $-1/\pi\text{Im}[\Sigma(\omega) + \Sigma_{\mathbf{k}}(\omega)]$ - additive local and "pseudogap" self-energies) corresponds to zero damping.
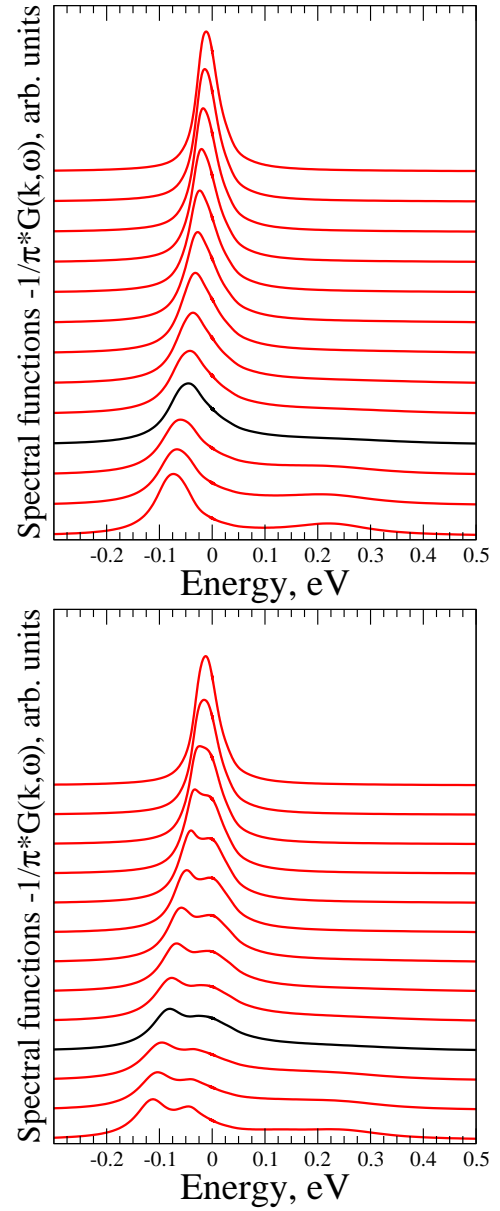
FIG. 5: (Color online) LDA+DMFT+$\Sigma_{\mathbf{k}}$ spectral densities for Bi2212 along of noninteracting FS in 1/8 of BZ for LDA-calculated value of $t_\perp$=0.03 eV (upper panel) and experimental value of $t_\perp^{exp}$=0.083 eV (lower panel) (Coulomb interaction U=1.51 eV, filling n=0.85, pseudogap potential Δ=0.21 eV, correlation length $\xi = 5a$).
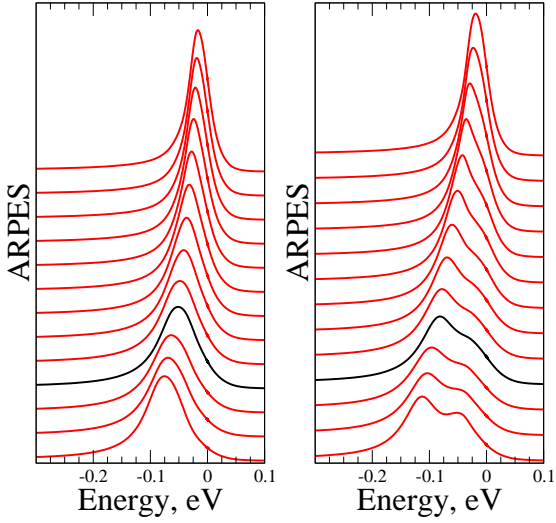
FIG. 6: (Color online) LDA+DMFT+$\Sigma_{\mathbf{k}}$ ARPES spectra for Bi2212 along of noninteracting FS in 1/8 of BZ for LDA-calculated value of $t_{\perp}$=0.03 eV (left) and experimental value of $t_{\perp}^{exp}$=0.083 eV (right). (Coulomb interaction U=1.51 eV, filling n=0.85, pseudogap potential Δ=0.21 eV, correlation length $\xi = 5a$). Corresponding spectral function $A(\omega, \mathbf{k})$ is multiplied with Fermi function at T~255K (the temperature of NRG calculations).
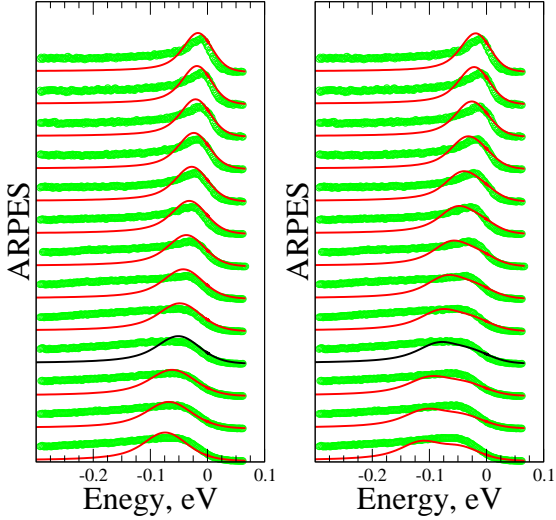

FIG. 7: (Color online) Comparison of LDA+DMFT+$\Sigma_{\mathbf{k}}$ ARPES spectra (solid lines) for Bi2212 along of noninteracting FS in 1/8 of BZ for LDA-calculated value of $t_{\perp}$=0.03 eV (left) and experimental value of $t_{\perp}^{exp}$=0.083 eV (right) with experimental ARPES (Ref.[59]) (circles). (Coulomb interaction U=1.51 eV, filling n=0.85, pseudogap potential Δ=0.21 eV, correlation length $\xi = 5a$). Corresponding spectral function $A(\omega, \mathbf{k})$ is multiplied by Fermi function at T=140K (the temperature of experiment) and broadened with Gaussian to simulate experimental resolution of 16 meV (Ref.[59]).
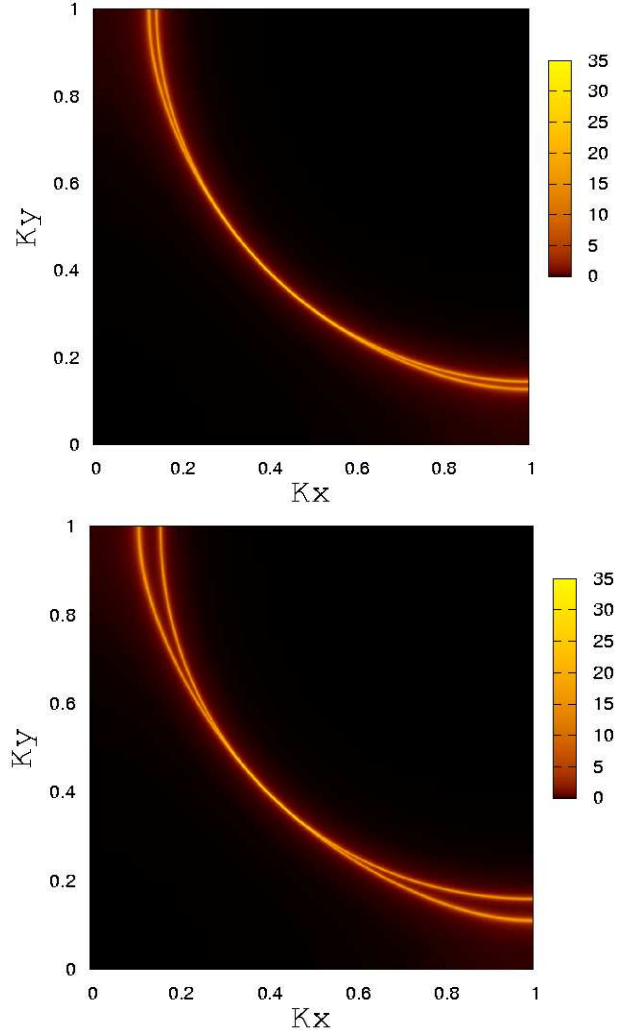

FIG. 8: (Color online) LDA+DMFT Fermi surfaces for Bi2212 within 1/4 of BZ (k_x, k_y in units of π/a) for LDA-calculated value of $t_{\perp}$=0.03 eV (upper panel) and experimental value of $t_{\perp}^{exp}$=0.083 eV (lower panel) (Coulomb interaction U=1.51 eV, filling n=0.85).
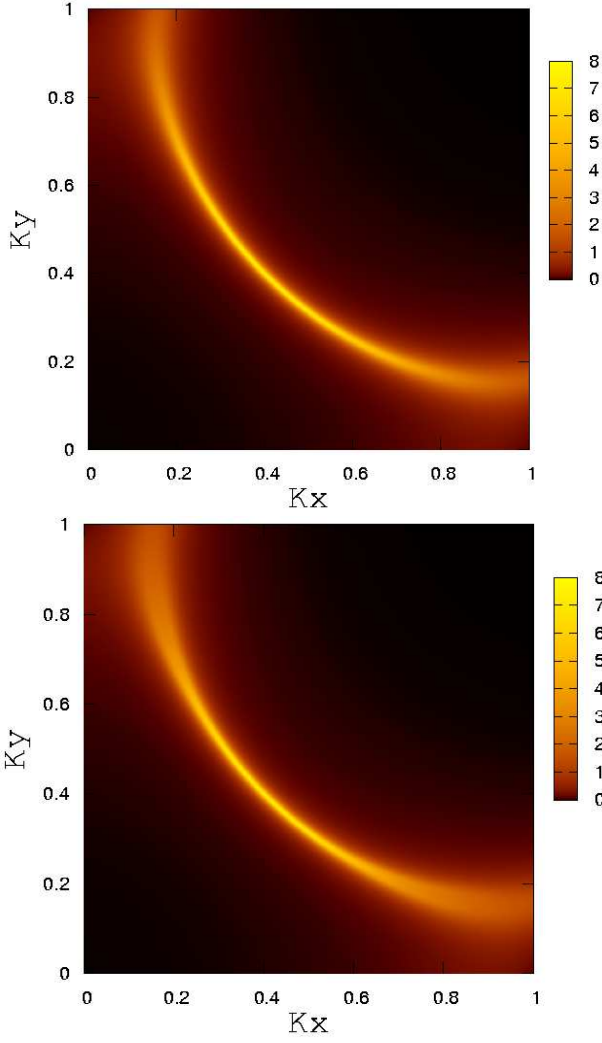
FIG. 10: (Color online) Comparison of experimental and theoretical LDA+DMFT+$\Sigma_{\mathbf{k}}$ static scattering $a(\mathbf{k}) = -1/\pi \mathrm{Im}\Sigma(0) + \Sigma_{\mathbf{k}}(0)$ for Bi2212 within 1/8 of BZ for LDA-calculated value of $t_{\perp}$=0.03 eV (light curve) and experimental value of $t_{\perp}^{exp}$=0.083 eV (dark curve) (Coulomb interaction U=1.51 eV, filling n=0.85, pseudogap potential Δ=0.21 eV, correlation length $\xi = 5a$).

Tables

FIG. 9: (Color online) LDA+DMFT+$\Sigma_{\mathbf{k}}$ Fermi surfaces for Bi2212 within 1/4 of BZ (k_x, k_y in inits of π/a) for LDA-calculated value of $t_{\perp}$=0.03 eV (upper panel) and experimental value of $t_{\perp}^{exp}$=0.083 eV (lower panel) (Coulomb interaction U=1.51 eV, filling n=0.85, pseudogap potential Δ=0.21 eV, correlation length $\xi = 5a$).

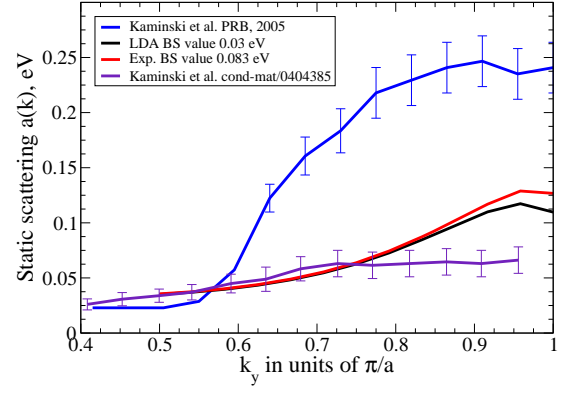TABLE I: Calculated energetic model parameters for Bi2212 (eV). First four Cu-Cu inplain hopping integrals t, t', t'', t''', interplain hopping value $t_{\perp}$, local Coulomb interaction U and pseudogap potential Δ.

t	t'	t''	t'''	$t_{\perp}$	U	Δ
-0.627	0.133	0.061	-0.015	0.03	1.51	0.21